



LJMU Research Online

Rodrigues, GB, Brancini, GTP, Uyemura, SA, Bachmann, L, Wainwright, M and Braga, GUL

Chemical features of the photosensitizers new methylene blue N and S137 influence their subcellular localization and photoinactivation efficiency in *Candida albicans*.

<http://researchonline.ljmu.ac.uk/id/eprint/13270/>

Article

Citation (please note it is advisable to refer to the publisher's version if you intend to cite from this work)

Rodrigues, GB, Brancini, GTP, Uyemura, SA, Bachmann, L, Wainwright, M and Braga, GUL (2020) Chemical features of the photosensitizers new methylene blue N and S137 influence their subcellular localization and photoinactivation efficiency in *Candida albicans*. *Journal of Photochemistry*

LJMU has developed **LJMU Research Online** for users to access the research output of the University more effectively. Copyright © and Moral Rights for the papers on this site are retained by the individual authors and/or other copyright owners. Users may download and/or print one copy of any article(s) in LJMU Research Online to facilitate their private study or for non-commercial research. You may not engage in further distribution of the material or use it for any profit-making activities or any commercial gain.

The version presented here may differ from the published version or from the version of the record. Please see the repository URL above for details on accessing the published version and note that access may require a subscription.

For more information please contact researchonline@ljmu.ac.uk

<http://researchonline.ljmu.ac.uk/>

1 Chemical features of the photosensitizers new methylene blue N and S137 influence their
2 subcellular localization and photoinactivation efficiency in *Candida albicans*

3

4

5

6 Gabriela Braga Rodrigues^{a,§}, Guilherme Thomaz Pereira Brancini^{a,§}, Sérgio Akira
7 Uyemura^a, Luciano Bachmann^b, Mark Wainwright^c, Gilberto Ubida Leite Braga^{a,*}

8

9

10

11 ^aDepartamento de Análises Clínicas, Toxicológicas e Bromatológicas, Faculdade de
12 Ciências Farmacêuticas de Ribeirão Preto, Universidade de São Paulo, Ribeirão Preto,
13 SP 14040-903, Brazil

14 ^bDepartamento de Física, Faculdade de Filosofia, Ciências e Letras de Ribeirão Preto.
15 Universidade de São Paulo, Ribeirão Preto, SP 14040-903, Brazil

16 ^cSchool of Pharmacy and Biomolecular Sciences, Liverpool John Moores University,
17 Liverpool L3 3AF, United Kingdom

18

19 ^{*}Corresponding author: Faculdade de Ciências Farmacêuticas de Ribeirão Preto,
20 Universidade de São Paulo, Ribeirão Preto, São Paulo, 14040-903, Brazil.

21 E-mail adress: gbraga@fcfrp.usp.br.

22 [§]These authors contributed equally to this work.

23

24 **ABSTRACT**

25 Antimicrobial photodynamic treatment (APDT) has emerged as an effective
26 therapy against pathogenic fungi with both acquired and intrinsic resistance to commonly
27 used antifungal agents. Success of APDT depends on the availability of effective
28 photosensitizers capable of acting on different fungal structures and species. Among the
29 phenothiazinium dyes tested as photoantifungals, new methylene blue N (NMBN) and
30 the novel pentacyclic compound S137 are the most efficient. In the present study we
31 compared the effects of APDT with NMBN and S137 on the survival of *Candida albicans*
32 and employed a set of fluorescent probes (propidium iodide, FUN-1, JC-1, DHR-123 and
33 DHE) together with confocal microscopy and flow cytometry to evaluate the effects of
34 these two chemically diverse photosensitizers on cell membrane permeability,
35 metabolism and redox status, and mitochondrial activity. Taken together, our results
36 indicate that, due to chemical features resulting in different lipophilicity, NMBN and
37 S137 localize to distinct subcellular structures and hence inactivate *C. albicans* cells via
38 different mechanisms. S137 localizes mostly to the cell membrane and, upon light
39 exposure, photo-oxidizes membrane lipids. NMBN readily localizes to mitochondria and
40 exerts its photodynamic effects there, which was observed to be a less effective way to
41 achieve cell death at lower light fluences.

42

43 **Keywords:** antimicrobial photodynamic treatment, fungal photodynamic inactivation,
44 phenothiazine photosensitizers, fluorescent probes, reactive oxygen species

45

46 1. Introduction

47 Several procedures in modern medicine, such as solid organ and hematopoietic
48 stem cell transplantations, surgeries, autoimmune disease therapies, and uncontrolled
49 HIV infection make millions of patients vulnerable to lethal fungal diseases (Köhler et al.
50 2015; Limper et al. 2017). *Candida albicans*, usually a harmless commensal fungus, is
51 also an opportunistic pathogen for immunocompromised people and the major human
52 fungal pathogen in the USA and several other countries (Nishimoto et al. 2020). Today,
53 fungal infections are among the most difficult diseases to treat in humans (Köhler et al.
54 2015). One of the factors that makes treatment so difficult is the rapid acquisition of
55 resistance to all of the only four major classes of antifungal agents clinically available:
56 azoles, polyenes, echinocandins, and a nucleotide analog (Chang et al. 2019; Perlin et al.
57 2017; Shor and Perlin 2015). Additionally, many species of *Candida*, such as *Candida*
58 *auris* and *Candida glabrata* are intrinsically resistant to some antifungal classes (Chang
59 et al. 2019; Nishimoto et al. 2020; Rhodes and Fisher 2019). Multidrug resistance can
60 eliminate treatment options completely, which has a serious effect on patient survival
61 (Perlin et al. 2017).

62 The emergence of resistance to currently used antifungals has promoted the
63 development of novel antifungal approaches, such as ~~the~~ antimicrobial photodynamic
64 treatment (APDT). The basic principle behind photodynamic antimicrobial inactivation
65 is the combination three factors: (1) visible or near-infrared light, (2) molecular oxygen,
66 and (3) a photosensitizer (PS). Light exposure excites the photosensitizer to a singlet state.
67 Then, intersystem crossing results in a photosensitizer in an excited triplet state which
68 can interact with molecular oxygen either via electron or energy transfer. Electron
69 transfer, also called Type I reactions, usually results in the formation of radicals such as
70 the superoxide radical anion. Conversely, energy transfer or Type II reaction results in

71 the formation of singlet oxygen. In either case, reactive oxygen species (ROS) such as
72 singlet oxygen, superoxide radical anions, and hydroxyl radicals have a broad spectrum
73 of activity and can damage several microbial targets ~~such as~~ among the various proteins,
74 lipids, and nucleic acids encountered, therefore making selection of resistant strains
75 unlikely (Brancini et al. 2016; Wainwright et al. 2017). Among photoantimicrobials
76 evaluated as antifungals, the phenothiazinium dyes methylene blue and toluidine blue are
77 the most commonly used, mainly due to their low toxicity and their long-established use
78 for other clinical applications (Rodrigues et al. 2013; Wainwright et al. 2017).
79 Phenothiazinium derivatives with improved photoantimicrobial activity against yeasts
80 and filamentous fungi such as new methylene blue N (NMBN) and the novel pentacyclic
81 compound S137, have been identified (Dai et al. 2011; Rodrigues et al. 2013). APDT
82 with NMBN and S137 has been shown to be highly effective against fungi of the genera
83 *Aspergillus* (de Menezes et al. 2014), *Candida* (Dai et al. 2011; Rodrigues et al. 2013),
84 *Colletotrichum* (de Menezes et al. 2014), *Neoscytalidium* (Tonani et al. 2018), and
85 *Trichophyton* (Rodrigues et al. 2012).

86 The most important factor determining the outcome of APDT is how a
87 photosensitizer interacts with cells of the target microorganism, with its subcellular
88 localization being of particular interest (Gonzales et al. 2017; de Menezes et al. 2014; de
89 Menezes et al. 2016). This is because ROS have a short half-life and therefore exert their
90 action in the vicinity of their production site (Castano et al. 2004). Cellular uptake and
91 intracellular localization is determined by chemical and structural features of the PS (e.g.
92 molecular mass, lipophilicity, charge distribution, number of H-bond donors and
93 acceptors, etc.), the concentration of the PS, the incubation time, and the phenotypic
94 characteristics of the target cells (Castano et al. 2004). PS characteristics such as charge

95 type and distribution as well as lipophilicity may be controlled by informed synthesis
96 (Wainwright and Giddens 2003).

97 The use of confocal laser scanning fluorescence microscopy has made the
98 determination of intracellular localization of PS much easier. Colocalization of
99 subcellular organelle-specific fluorescent probes with differing fluorescence emission
100 peak to that of the PS can be used to more closely identify the site of localization and
101 these probes can also be used to identify sites of damage after illumination (Castano et al.
102 2004).

103 The photosensitizers NMBN and S137 are chemically and structurally distinct,
104 and consequentially present different outcomes when used in APDT. For instance, use of
105 S137 usually results in cell damage even in the dark (dark toxicity) and its microbial
106 photoinactivation tends to be higher at lower light fluences when compared to NMBN.
107 As previously mentioned, PS subcellular localization can greatly influence the results of
108 APDT. Therefore, here we compared NMBN and S137 by employing a set of fluorescent
109 probes (propidium iodide, FUN-1, JC-1, DHR-123, and DHE) together with confocal
110 microscopy and flow cytometry in order to evaluate potential PS subcellular localization
111 as well as the mechanism behind APDT with these PS.

112

113 **2. Materials and Methods**

114 *2.1. C. albicans strain and growth conditions*

115 *C. albicans* strain ATCC 64548 was obtained from the American Type Culture
116 Collection (ATCC) (Manassas, USA). Cells were grown on Sabouraud Dextrose Agar
117 (SDA) medium (BD Difco, USA) in the dark, at 35 °C, for 48 h. Cells from isolated
118 colonies were transferred to 150-mL Erlenmeyer flasks containing 50 mL of YPD
119 medium [1% Yeast Extract (BD Difco, Sparks, USA), 2% Peptone (BD Difco) and 2%

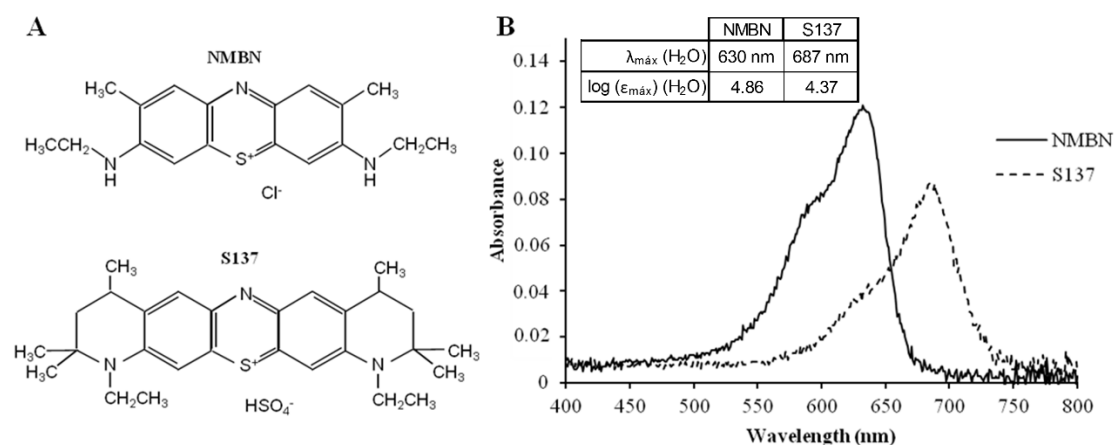
120 Dextrose (Vetec, Duque de Caxias, Brazil)]. Cultures were incubated in the dark at 35 °C
 121 for 6 h under shaking (100 rpm). Cells were then washed in phosphate-buffered saline
 122 (PBS, pH 7.4) (8,000 × g, 5 min) and cell concentration was adjusted by counting in a
 123 hemocytometer and performing the appropriate dilutions in PBS.

124

125 2.2. Photosensitizers

126 New Methylene Blue N zinc chloride double salt (NMBN) was purchased from
 127 Sigma-Aldrich (catalog number 202096; St. Louis, USA) (Fig. 1A). The pentacyclic
 128 phenothiazinium photosensitizer S137 was synthesized as previously described
 129 (Wainwright et al. 2011) (Fig. 1A). Stock solutions of the PS were prepared in water at a
 130 concentration (500 μM) two hundred-fold greater than the concentration used in the
 131 study. The solutions were stored in the dark at -20 °C for up to 2 weeks. Dilutions were
 132 prepared in PBS. Absorption spectra of the PS were obtained with a Ultrospec™ 2100
 133 Pro UV-visible spectrophotometer (GE Healthcare) in water (Fig. 1B).

134



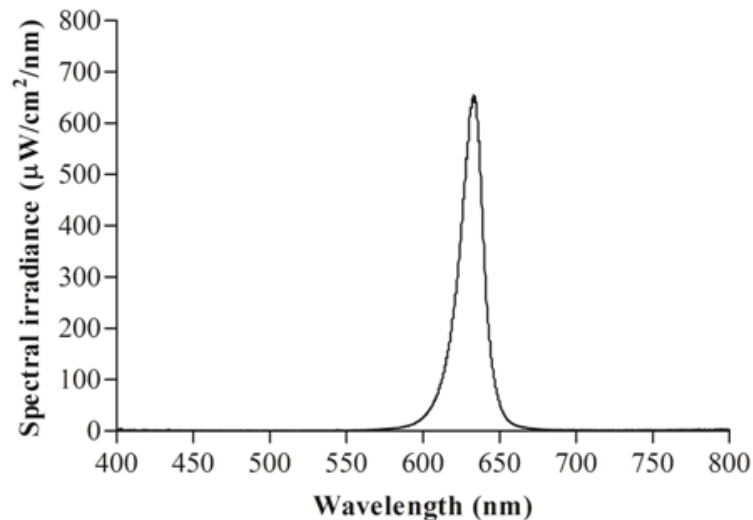
135

136 **Fig. 1.** Chemical structure (A) and absorption spectra (B) of the photosensitizers NMBN and S137

137

138 2.3. Light exposure

139 Light was provided by an array of 96 light-emitting diodes (LED) with peak
140 emission at 631 ± 20 nm and an irradiance of 13.89 mW cm^{-2} . Irradiance and emission
141 spectrum (Fig. 2) were obtained with a USB spectroradiometer (Ocean Optics, Dunedin,
142 USA) as previously described (Rodrigues et al. 2012).
143



144
145 **Fig. 1.** Irradiance spectrum of the red light source used in this study

146
147 *2.4. Photodynamic treatment*

148 Five mL of the fungal cell suspension and 5 mL of the PS (NMBN or S137) were
149 added to 15 mL tubes (TPP, Switzerland). Final concentrations of cells and PS in the
150 mixture were 2×10^7 cells mL^{-1} and $2.5 \mu\text{M}$ of NMBN or S137. Tubes were kept in the
151 dark for 30 min at 28°C and light exposure was performed under agitation in a 60-mm
152 Petri dish. The fluences used were 3, 9, and 14 J cm^{-2} (obtained after 3.42, 10.28, and
153 17.13 min, respectively). Relative cell survival after APDT was evaluated for each
154 fluence used by counting colony-forming units (CFU). To do this, the initial suspensions
155 were serially diluted tenfold in PBS to give dilutions of 10^{-1} to 10^{-3} . Fifty microliters were
156 then spread on the surface of 5 mL of SDA medium in Petri dishes (60×15 mm). Three

157 replicate-dishes were prepared for each light treatment. The dishes were incubated in the
158 dark at 35 °C. After 24 h, CFU were counted at 8× magnification daily for up to 4 days.
159 A dark control group was obtained by treating cells with PS but never exposing them to
160 light. A light control group was prepared by exposing cells alone (in the absence of PS)
161 to light fluences of 3, 9, and 14 J cm⁻². Absolute controls consisted of cells unexposed to
162 either light or PS. Relative survival was calculated as the ratio of CFU of fungal cells
163 treated only with light (light effect), only with PS (toxicity in the dark), and light and PS
164 (APDT) to CFU treated with neither light nor PS. Three independent experiments were
165 performed.

166

167 *2.5. Propidium iodide (PI) staining and visualization*

168 After APDT with NMBN or S137, cell suspensions were washed with PBS to
169 remove excess PS. Cells were then suspended in a 1.5 μM PI (Sigma-Aldrich, catalog
170 number P4170) solution prepared in PBS immediately before being used. Flow cytometry
171 was performed in a BD FACSCanto I equipment and BD FACSDiva software. In each
172 experiment, ten thousand events were monitored with excitation at 488 nm and detection
173 between 564 and 606 nm. Cells not treated with PS and cells treated with 70% ethanol
174 were used as negative and positive controls, respectively. Three independent experiments
175 were performed.

176 Confocal fluorescence microscopy was used to visualize PI entry into cells. After
177 APDT and PI staining, cells were centrifuged (10,000 × g, 2 min) and the supernatant was
178 discarded. Three microliters of 2% Ultra Pure low-melting-point agarose (Invitrogen) and
179 3 μL of Fluoromount (Sigma) were added to 3 μL of cell pellet and the mixture was used
180 to mount the slide. Confocal microscopy was performed on a Leica DMI 6000 CS,
181 scanner TCS SP8 with a 63× objective lens (f/1.4) and using oil immersion. For PI

182 visualization, excitation was performed with an Optically Pumped Semiconductor Laser
183 at 488 nm and detection at 597-637 nm.

184

185 *2.6. FUN-1 staining and visualization*

186 After APDT with NMBN or S137, cells were washed with 10 mM HEPES pH 7.2
187 (Sigma-Aldrich) supplemented with 2% glucose (hereinafter referred to as GH buffer) to
188 remove excess PS. Cells were then suspended in a 0.5 μ M FUN-1 solution (Molecular
189 Probes, Life Technologies, Eugene, OR, USA) prepared in GH buffer. Cells were
190 incubated in the dark under shaking (300 rpm) at 30 °C for 30 min. The
191 spectrofluorimetric analysis was performed in black 96-well plates with a Synergy 2
192 equipment (BioTek[®], Winooski, USA). Excitation was set to 475-495 nm and detection
193 to 518-538 nm (green fluorescence) and 580-600 nm (red fluorescence). Three
194 independent experiments were performed.

195 For confocal microscopy, FUN-1-stained cells were centrifuged (10,000 \times g, 2
196 min) and slides were mounted and visualized as described above for PI. Laser excitation
197 was set to 488 nm and detection to 530-560 nm (green fluorescence) and 604-636 nm (red
198 fluorescence).

199

200 *2.7. JC-1 staining and visualization*

201 After APDT with NMBN and S137, cells were washed (10,000 \times g, 2 min) with
202 GH buffer to remove excess PS. Cells were then suspended in a 5 μ M JC-1 (Molecular
203 Probes, Life Technologies, USA) solution prepared in GH buffer and incubated in the
204 dark under shaking (300 rpm) at 35 °C for 30 min. Then, cells were washed twice with
205 GH buffer and flow cytometry was performed as described previously. A total of 10,000
206 events were monitored. Excitation was set to 488 nm and detection to 515-545 nm (green

207 fluorescence) and 564-606 nm (red fluorescence). Three independent experiments were
208 performed.

209 Confocal microscopy was performed as described previously. Laser excitation
210 was set to 488 nm and detection to 505-550 nm (green fluorescence) and 575-630 (red
211 fluorescence).

212

213 *2.8. Dihydrorhodamine-123 (DHR-123) staining and visualization*

214 After APDT with NMBN or S137, cells were washed ($10,000 \times g$, 2 min) with
215 GH buffer to remove excess PS. Cells were then suspended in a $5 \mu\text{g mL}^{-1}$ DHR-123
216 solution (Sigma-Aldrich, catalog number D1054) prepared in GH buffer and incubated in
217 the dark at 25°C for 120 min. Flow cytometry was performed as described previously. A
218 total of 10,000 events were monitored. Excitation was set to 488 nm and detection to 515-
219 545 nm. Three independent experiments were performed.

220 Confocal microscopy was performed as described previously. Laser excitation
221 was set to 488 nm and detection to 501-570 nm.

222

223 *2.9. Dihydroethidium (DHE) staining and visualization*

224 After APDT with NMBN or S137, cells were washed ($10,000 \times g$, 2 min) with
225 GH buffer to remove excess PS. Cells were then suspended in a $20 \mu\text{M}$ DHE (Sigma-
226 Aldrich, catalog number D7008) solution prepared in GH buffer and incubated in the dark
227 at 25°C for 45 min. Flow cytometry was performed in a Guava EasyCyte 8HT (Merck
228 Millipore, Darmstadt, Germany). In each experiment, a total of 30,000 events were
229 analyzed using the red filter. Three independent experiments were performed.

230 Confocal microscopy was performed as described previously. Laser excitation
231 was set to 552 nm and detection to 556-624 nm.

232

233 *2.10. PS lipophilicity prediction*

234 Lipophilicity of NMBN and S137 (as expressed by logD as a function of pH) was
235 calculated with the MarvinJS logD Predictor software (ChemAxon). PS structures used
236 in the predictions are those depicted in Fig. 1.

237

238 *2.11. Statistical analysis*

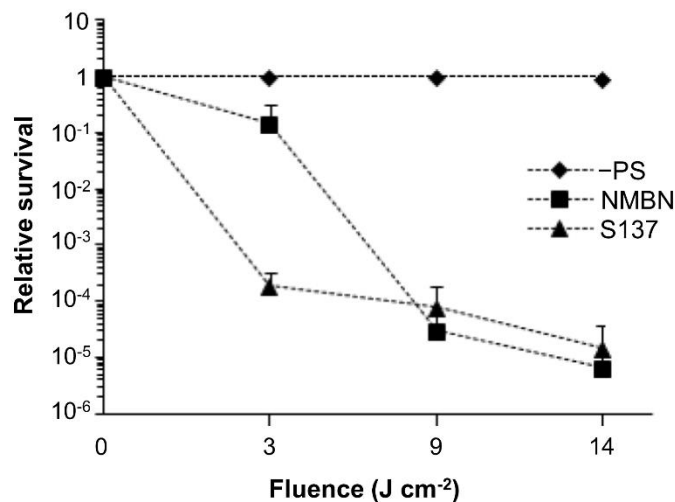
239 Differences between means were analyzed via ANOVA with Tukey's post-test.
240 Significance threshold was set to $P < 0.05$. Statistical analyses were performed with SAS®
241 9.2 software (SAS Analytics, USA).

242

243 **3. Results**244 *3.1. C. albicans survival after APDT*

245 The PS NMBN and S137 were compared in terms of cell mortality after APDT
246 with fluences of 3, 9, and 14 J cm⁻². Importantly, treatment with PS alone or light exposure
247 alone did not result in cell mortality (Fig. 3). At 3 J cm⁻², S137 was a much more effective
248 PS, reducing cell viability by 99.98% (3.70 log₁₀) whereas NMBN achieved only 85.2%
249 (0.83 log₁₀) under the same conditions (Fig. 3). Increasing fluence to 9 and to 14 J cm⁻²
250 allowed NMBN and S137 to achieve similar cell mortality, which was above four orders
251 of magnitude for both PS (Fig. 3).

252



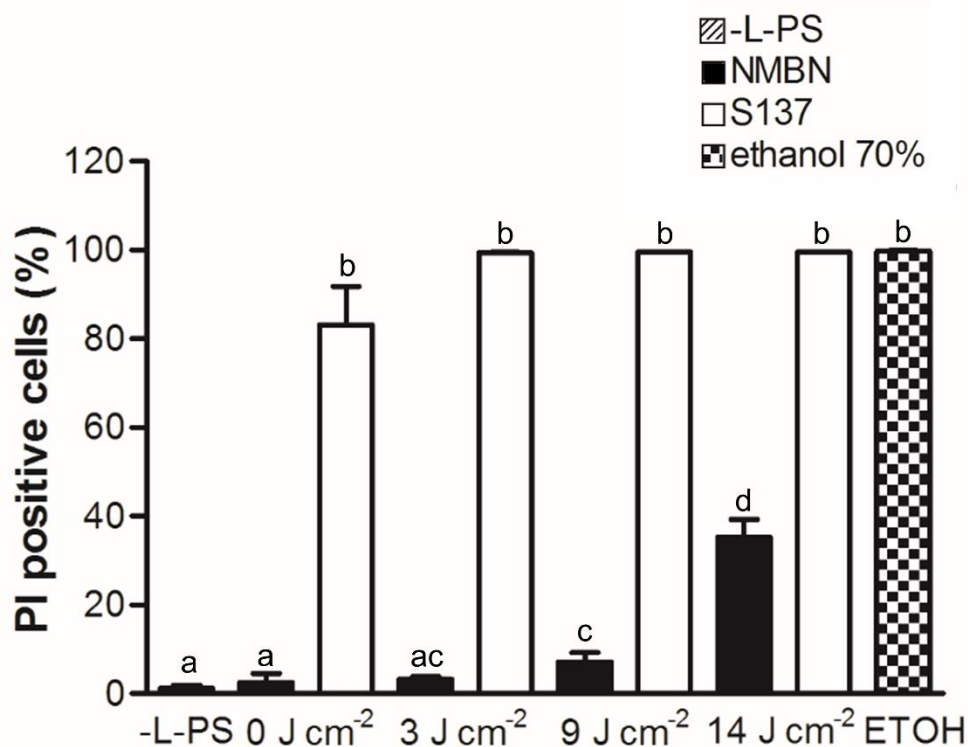
253

254 **Fig. 3.** Relative survival of *Candida albicans* after antimicrobial photodynamic treatment
 255 with NMBN and S137 as a function of light fluence. Control groups were either treated
 256 with light alone (-PS) or photosensitizer alone (fluence = 0 J cm⁻²). Error bars are the
 257 standard deviation from three independent experiments.

258

259 3.2. Propidium iodide staining and visualization

260 Staining with PI was used to study fungal membrane disturbance caused by the
 261 PS both in the dark and after APDT. In the dark, NMBN caused little to no PI labeling as
 262 evaluated by flow cytometry whereas S137 caused about 80% of cells to become PI-
 263 positive (Fig. 4). The percentage of PI-positive cells achieved 100% for S137 already at
 264 the lowest fluence used (3 J cm⁻²) whereas this number was only about 40% for NMBN
 265 even at the highest fluence (14 J cm⁻²) (Fig. 4).



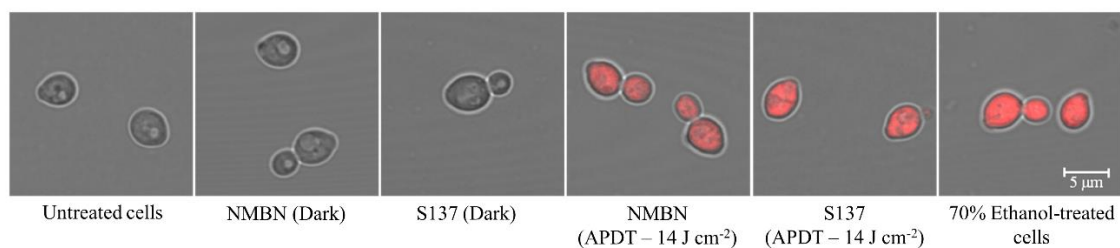
266

267 **Fig. 4.** *Candida albicans* Propidium iodide staining as evaluated by flow cytometry. Cells
 268 were treated with either NMBN or S137 and control groups received neither light nor
 269 photosensitizer (-L -PS). Different lower case letters indicate that means are statistically
 270 different. Error bars are the standard deviation from three independent experiments.

271

272 Although adding S137 resulted in PI permeability already in the dark in flow
 273 cytometry experiments, confocal fluorescence microscopy could not distinguish between
 274 NMBN and S137 in the dark (Fig. 5). At 14 J cm⁻², both NMBN- and S137-treated cells
 275 were stained (Fig. 5).

276



277

278 **Fig. 5.** *Candida albicans* propidium iodide staining as evaluated by confocal fluorescence
 279 microscopy. Control cells were not treated with either photosensitizer or light. NMBN

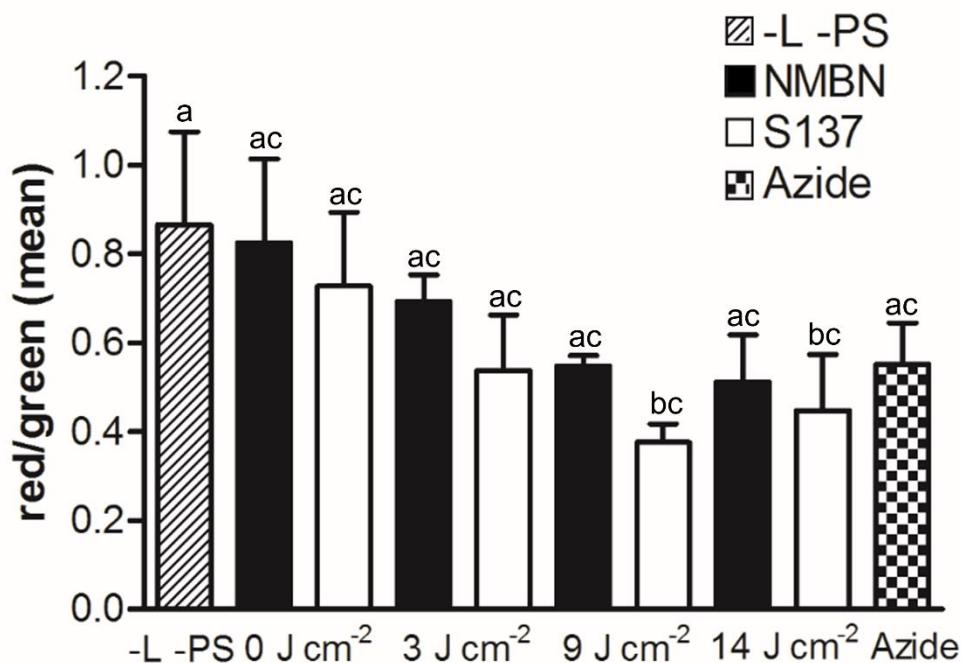
280 and S137 were used either in the dark or under light at a fluence of 14 J cm⁻². Images are
 281 representative of three independent experiments.

282

283 3.3. FUN-1 staining and visualization

284 FUN-1 is a dye that diffuses inside fungal cells and stains them green irrespective
 285 of viability. However, in viable cells, further processing of the dye results in the
 286 appearance of red fluorescent spots accompanied by reduced green fluorescence.
 287 Therefore, the red/green fluorescence ratio is used as a marker of cell viability in flow
 288 cytometry experiments. Cells treated with either NMBN or S137 in the dark were not
 289 significantly different from untreated cells (Fig. 6). After APDT, the red/green
 290 fluorescence ratio decreased proportionally with increasing fluences and both PS were
 291 similar in this regard, although the majority of differences were not statistically
 292 significant (Fig. 6).

293



294

295 **Fig. 6.** *Candida albicans* FUN-1 staining as evaluated by spectrofluorimetry. Cells were
 296 treated with either NMBN or S137 and control groups received neither light nor

297 photosensitizer (-L -PS). Different lower case letters indicate that means are statistically
 298 different. Error bars are the standard deviation from three independent experiments.

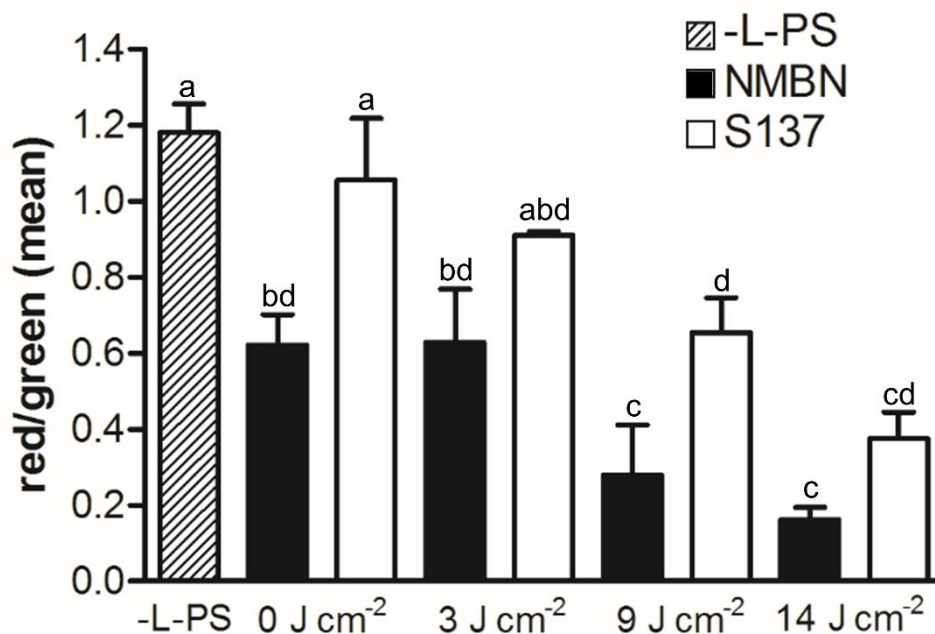
299

300 As expected, confocal fluorescence microscopy showed the accumulation of
 301 vacuolar-like red fluorescence in untreated cells and those that were treated with either
 302 PS in the dark, indicating normal viability (Fig. S1). After APDT with 14 J cm^{-2} , these
 303 red spots were lost and cells stained yellow (Fig. S1).

304

305 3.4. JC-1 staining and visualization

306 JC-1 is a dye that accumulates in mitochondria in a membrane potential-dependent
 307 manner. This accumulation is indicated by a red-to-green fluorescence shift. The loss of
 308 mitochondrial membrane potential (depolarization) reduces the red/green fluorescence
 309 ratio. Treating cells with S137 in the dark resulted in no mitochondria depolarization.
 310 However, NMBN caused considerable loss of membrane potential in the dark (Fig. 7).



311

312 **Fig. 7.** *Candida albicans* JC-1 staining as evaluated by flow cytometry. Cells were treated
 313 with either NMBN or S137 and control groups received neither light nor photosensitizer
 314 (-L -PS). Different lower case letters indicate that means are statistically different. Error
 315 bars are the standard deviation from three independent experiments

316

317 Mitochondrial membrane potential decreased upon light exposure for both PS,
318 even though S137 required a fluence of 9 J cm^{-2} to achieve a statistically significant
319 difference from the control (Fig. 7).

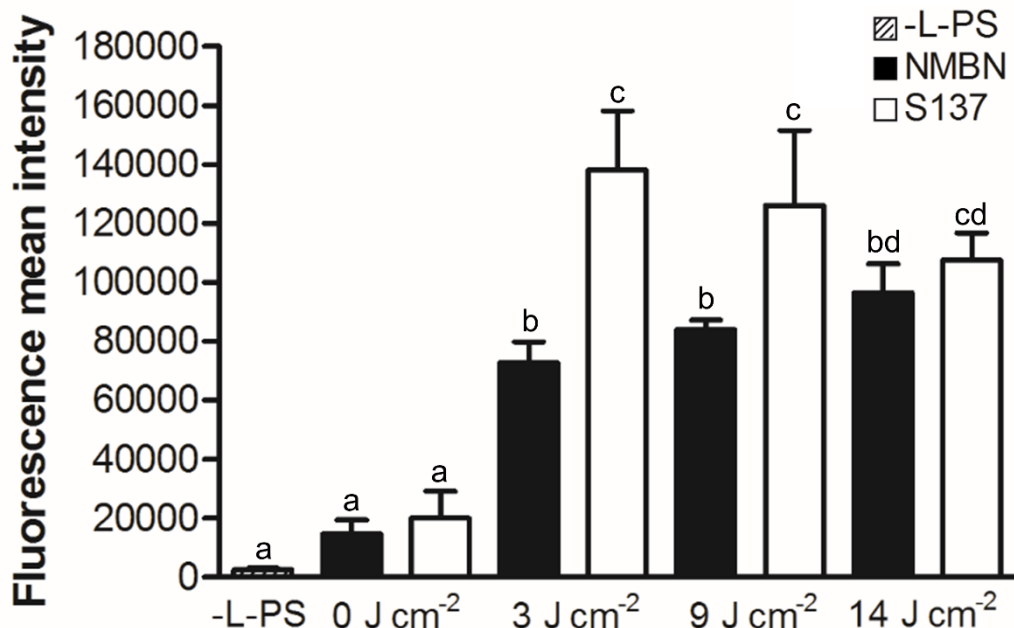
320 Although flow cytometry experiments showed that NMBN can reduce
321 mitochondrial membrane potential already in the dark, fluorescence microscopy did not
322 indicate the same result as both NMBN and S137, when used in the dark, were very
323 similar to untreated cells (Fig. S2). Upon light exposure (14 J cm^{-2}), the expected decrease
324 in red/green fluorescence ratio was observed for both PS. However, loss of red
325 fluorescence was higher for NMBN when compared to S137 (Fig. S2), which reflects
326 flow cytometry experimental data (Fig. 7).

327

328 *3.5. Dihydrorhodamine-123 (DHR-123) staining and visualization*

329 DHR-123 is an uncharged and membrane-permeant compound that, upon
330 oxidation, is converted to the mitochondrial dye rhodamine-123, emitting green
331 fluorescence. Treating cells with either PS in the dark did not result in a significant
332 increase in green fluorescence. Light exposure at a fluence of 3 J cm^{-2} revealed that S137
333 generated more DHR-123-oxidizing species than did NMBN (Fig. 8), which was also
334 observed for the fluence of 9 J cm^{-2} . At 14 J cm^{-2} , both PS leveled off and produced about
335 the same amount of oxidizing species (Fig. 8).

336



337

338 **Fig. 8.** *Candida albicans* Dihydrorhodamine-123 staining as evaluated by flow
 339 cytometry. *Candida albicans* cells were treated with either NMBN or S137 and control
 340 groups received neither light nor photosensitizer (-L -PS). Different lower case letters
 341 indicate that means are statistically different. Error bars are the standard deviation from
 342 three independent experiments.

343

344 Fluorescence microscopy, as expected, showed no green fluorescence in untreated
 345 cells and cells treated with either PS (Fig. S3). Strong green fluorescent emission was
 346 observed at 14 J cm⁻², which was similar for NMBN and S137 (Fig. S3).

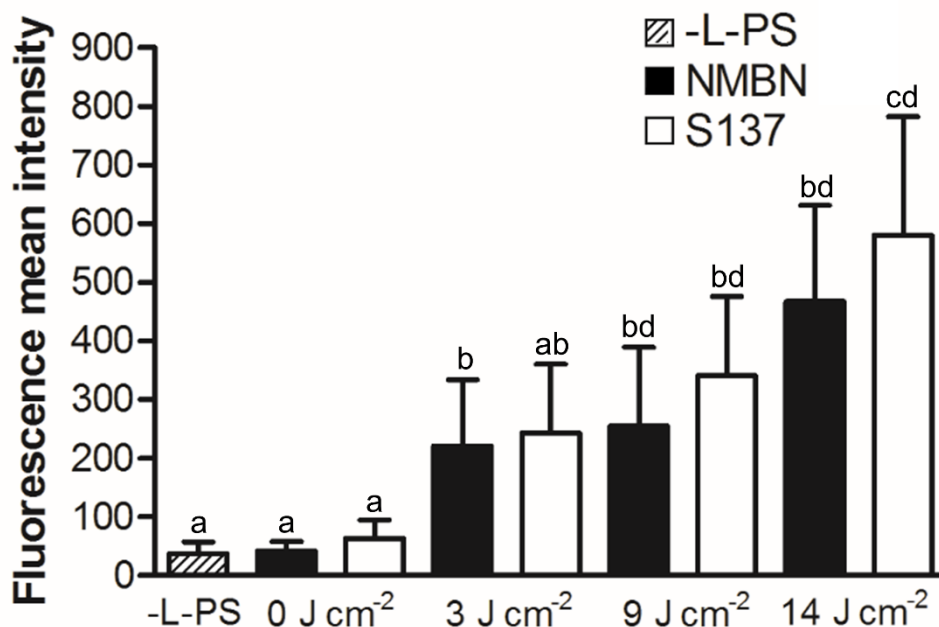
347

348 3.6. Dihydroethidium (DHE) staining and visualization

349 DHE is widely regarded as an indicator of superoxide anion radical (O₂^{•-})
 350 production because DHE oxidation by O₂^{•-} gives 2-hydroxyethidium, which emits red
 351 fluorescence. However, unspecific oxidation of DHE by other ROS results in ethidium,
 352 which also emits red fluorescence and is hard to distinguish from 2-hydroxyethidium.
 353 Therefore, we employed DHE as a general indicator of ROS and not specifically of O₂^{•-}.
 354 Neither NMBN nor S137 leads to ROS production in the dark when compared to

355 untreated cells (Fig. 9). ROS production increased upon light exposure, although we
 356 observed no difference between NMBN and S137 (Fig. 9).

357



358

359 **Fig. 9.** *Candida albicans* dihydroethidium staining as evaluated by flow cytometry. Cells
 360 were treated with either NMBN or S137 and control groups received neither light nor
 361 photosensitizer (-L -PS). Different lower case letters indicate that means are statistically
 362 different. Error bars are the standard deviation from three independent experiments.

363

364 Confocal fluorescence microscopy reflected flow cytometry results: no red
 365 fluorescence was observed in the dark for either PS and red fluorescence was observed at
 366 14 J cm⁻² that was indistinguishable between NMBN and S137 (Fig. S4).

367

368 3.7. NMBN and S137 lipophilicity prediction

369 In the dark, S137 caused extensive membrane damage (Fig. 4) and NMBN
 370 reduced mitochondrial membrane potential (Fig. 7). These observations prompted an
 371 investigation of PS lipophilicity. Predicting logD as a function of pH for both PS revealed
 372 that whereas NMBN is of moderate lipophilicity (logD = 3.08 at pH 7), S137 is highly

373 lipophilic ($\log D = 6.26$) (Fig. 10A). For comparison, we also calculated $\log D$ values for
374 the membrane component ergosterol ($\log D = 6.63$) and the mitochondria-specific dye
375 MitoTracker™ Red CMXRos ($\log D = 2.72$) (Fig. 10B).

376

384 4. Discussion

385 Understanding the mechanism behind microbial photoinactivation with different
386 PS is a key step in improving the efficiency of APDT and in selecting the most appropriate
387 PS based on target microorganism and condition. APDT of *C. albicans* with the PS
388 NMBN and S137 revealed that the latter achieves increased cell mortality at lower
389 fluences when compared to the former (Fig. 3). Under the experimental conditions used
390 here, NMBN is expected to produce more singlet oxygen compared to S137 as its peak
391 absorption (630 nm, Fig. 1B) essentially matches that of the light system used (631 nm).
392 Furthermore, NMBN has a higher molar absorption coefficient (Fig. 1B). Indeed, recent
393 observations from our group have shown that singlet oxygen quantum yield of NMBN is
394 higher than that of S137 (De Menezes et al., in preparation). Therefore, the different
395 efficiency in APDT between NMBN and S137 at 3 J cm^{-2} cannot be explained by
396 photophysical properties alone. To better understand this phenomenon, we employed a
397 set of fluorescent dyes analyzed by both flow cytometry (or spectrofluorimetry in the case
398 of FUN-1) and confocal fluorescence microscopy.

399 Initially, we used FUN-1 and PI as vital dyes. FUN-1 was not capable of
400 distinguishing the difference between APDT with NMBN and S137 at 3 J cm^{-2} (Fig. 6),
401 showing that it is not an adequate dye to evaluate cell mortality after APDT. Results
402 obtained with PI showed that S137 caused extensive membrane permeabilization even in
403 the dark whereas NMBN could only permeabilize the membrane at higher light fluences
404 (Fig. 4). Interestingly, membrane permeabilization by S137 was unrelated to cell survival
405 as this PS caused no mortality in the dark (Fig. 3). This is in agreement with prior works
406 showing that membranes of stressed yeast and conidia of filamentous fungi can become
407 permeable to PI without loss of cell viability (Davey and Hexley 2011; de Menezes et al.
408 2016; Tonani et al. 2018).

409 The above-mentioned increase in PI permeability after S137 treatment in the dark
410 was easily quantified by flow cytometry (Fig. 4) but was not observed by confocal
411 fluorescence microscopy (Fig. 5). This discrepancy between the two techniques is likely
412 a consequence of differences in sensitivity. Flow cytometry is more sensitive than
413 confocal microscopy because, in the latter, out-of-focus image signals are ignored by the
414 confocal system, rendering this technique inadequate for faint fluorescence probes (Basiji
415 et al. 2007). On the other hand, flow cytometry sacrifices all imaging capabilities in favor
416 of greater sensitivity. In fact, flow cytometry can detect as few as 100 fluorescent
417 molecules per cell (Basiji et al. 2007), making it the method of choice for quantitative
418 measurement of a heterogeneous population of cells. Therefore, we can hypothesize that
419 confocal microscopy could not detect the difference between NMBN and S137 in the dark
420 for PI because the number of PI molecules entering the cell in S137-treated samples is
421 insufficient to produce a fluorescence signal that is strong enough to be detected by
422 confocal microscopy. Further evidence of this difference in sensitivity is that for other
423 fluorescent probes (such as DHR-123) confocal microscopy fails to detect any fluorescent
424 signal for both PS in the dark whereas flow cytometry detects a weak signal.

425 The increased uptake of PI by S137-treated cells prompted us to investigate PS
426 lipophilicity. Predicting logD for S137 and NMBN revealed that the former is about
427 1,500-fold more lipophilic than the latter at pH 7 (Fig. 10A). Indeed, S137 has a logD
428 value comparable to that of ergosterol (Fig. 10B). These results indicate that S137 mainly
429 accumulates at the cell membrane, potentially disturbing it and subsequently increasing
430 PI permeability.

431 On the other hand, NMBN is only moderately lipophilic, which, combined with
432 its positive charge, makes the PS a good candidate for mitochondria targeting (Rashid
433 and Horobin 1990). Accordingly, the lipophilicity of NMBN is comparable to that of the

434 mitochondria-specific dye MitoTracker™ Red CMXRos (Fig. 10B). Use of the
435 mitochondrial membrane potential indicator JC-1 revealed that NMBN caused
436 considerable membrane depolarization already in the dark whereas S137 treatment was
437 not different from untreated cells (Fig. 7). The fact that S137 is also a lipophilic cationic
438 compound could indicate that it also targets mitochondria. However, extremely lipophilic
439 compounds can take as long as hours or even days to diffuse through the lipid bilayer, a
440 task that is achieved within minutes for moderately lipophilic molecules (Baláz 2000;
441 Rashid and Horobin 1990). Therefore, under our experimental conditions in which cells
442 and PS were allowed to interact for 30 min, the most likely outcome is that NMBN
443 accumulates in mitochondria while S137, owing to its very high lipophilicity, is trapped
444 at the cell membrane.

445 The reduced mitochondrial membrane potential observed after NMBN treatment
446 could affect the outcome of some commonly used fluorescent dyes for monitoring
447 reactive species production. This is the case for DHR-123. Oxidation of DHR-123
448 produces rhodamine-123 which localizes to mitochondria. However, rhodamine-123
449 accumulation is dependent on mitochondrial status: loss of membrane potential reduces
450 dye accumulation and therefore washes away the fluorescent signal (Scaduto and
451 Grotyohann 1999). In our experiments, rhodamine-123 signal was increased for S137 at
452 3 J cm^{-2} when compared to NMBN, which would be a plausible explanation for the higher
453 mortality achieved by S137 (Fig. 8). However, this result needs to be interpreted with
454 care. Because NMBN caused mitochondrial membrane depolarization already in the dark,
455 then rhodamine-123 accumulation and signal could be hindered in NMBN-treated cells.
456 In support of this hypothesis, rhodamine-123 fluorescence did not increase for either S137
457 or NMBN when fluence increased (Fig. 8), probably as a consequence of the reduced
458 mitochondrial membrane potential at higher fluences (Fig. 7).

459 To overcome this limitation, we used DHE as a marker for the production of
460 reactive species as it does not depend on mitochondrial status. The fact that NMBN and
461 S137 produced approximately the same amount of reactive species at all light fluences
462 tested (Fig. 9) indicates that it is most likely PS subcellular localization, and not the
463 amount of reactive species generated, the deciding factor for APDT efficiency under our
464 experimental conditions. In support of this hypothesis, prior work evaluating a series of
465 photophysically similar porphyrin PS reported that photodynamic efficiency increases
466 with increasing membrane binding and is only partially dependent on mitochondria
467 localization (Pavani et al. 2009). Also, for PS targeting mitochondria, loss of membrane
468 potential resulted in decreased binding (Pavani et al. 2009), a feature that could affect the
469 outcome of APDT employing mitochondria-targeting PS such as NMBN.

470

471 **5. Conclusion**

472 Taken together, our results indicate that S137 and NMBN localize to different
473 subcellular structures and hence inactivate *C. albicans* cells via different mechanisms.
474 S137 localizes mostly to cell membrane and, upon light exposure, photo oxidizes
475 membrane lipids, which in turn could change membrane permeability to S137 itself and
476 allow the PS to reach other intracellular sites (Bocking et al. 2000). On the other hand,
477 NMBN readily localizes to mitochondria and exerts its photodynamic effects there, which
478 was observed to be a less effective way to achieve cell death at lower fluences. Finally,
479 while using a combination of fluorescent dyes allowed us to better comprehend APDT
480 with two distinct PS, the use of individual stains could be problematic: FUN-1 as a vital
481 stain could not tell apart the differences in survival between S137 and NMBN at 3 J cm^{-2} ,
482 ², DHR-123 depends on mitochondrial status which was affected by NMBN in the dark;
483 and DHE is only a general indicator of reactive species production and cannot take into

484 account that the same species could differently affect survival depending on where it is
485 generated.

486

487 **Acknowledgments**

488 We thank Eduardo Tozatto and Fabiana Rossetto de Moraes, both from Faculdade de
489 Ciências Farmacêuticas de Ribeirão Preto, for confocal microscopy and flow cytometry
490 analyses, respectively. This work was supported by the State of São Paulo Research
491 Foundation (FAPESP) grants 2012/15204-8 and 2016/11386 as well as by the National
492 Council for Scientific and Technological Development (CNPq) grants 425998/2018-5
493 and 307738/2018-3 to G.UL.B. We sincerely thank FAPESP for a post-doc fellowship to
494 G.B.R. (2012/22933-6) and for a Ph.D. scholarship to G.T.P.B. (2015/24305-0).

495

496 **REFERENCES**

- 497 Baláž, Š., 2000 Lipophilicity in trans-bilayer transport and subcellular pharmacokinetics.
498 *Perspectives in Drug Discovery and Design* 19:157-177.
- 499 Basiji, D.A., W.E. Ortyń, L. Liang, V. Venkatachalam, and P. Morrissey, 2007 Cellular
500 image analysis and imaging by flow cytometry. *Clin Lab Med* 27 (3):653-670,
501 viii.
- 502 Bocking, T., K.D. Barrow, A.G. Netting, T.C. Chilcott, H.G. Coster *et al.*, 2000 Effects
503 of singlet oxygen on membrane sterols in the yeast *Saccharomyces cerevisiae*.
504 *Eur J Biochem* 267 (6):1607-1618.
- 505 Brancini, G.T., G.B. Rodrigues, M.S. Rambaldi, C. Izumi, A.P. Yatsuda *et al.*, 2016 The
506 effects of photodynamic treatment with new methylene blue N on the *Candida*
507 *albicans* proteome. *Photochem Photobiol Sci* 15 (12):1503-1513.
- 508 Castano, A.P., T.N. Demidova, and M.R. Hamblin, 2004 Mechanisms in photodynamic
509 therapy: part one—photosensitizers, photochemistry and cellular localization.
510 *Photodiagnosis Photodyn Ther* 1 (4):279-293.
- 511 Chang, Z., V. Yadav, S.C. Lee, and J. Heitman, 2019 Epigenetic mechanisms of drug
512 resistance in fungi. *Fungal Genet Biol* 132:103253.
- 513 Dai, T., V.J. Bil de Arce, G.P. Tegos, and M.R. Hamblin, 2011 Blue Dye and Red Light,
514 a Dynamic Combination for Prophylaxis and Treatment of Cutaneous *Candida*
515 *albicans* Infections in Mice. *Antimicrob Agents Chemother* 55 (12):5710-5717.
- 516 Davey, H.M., and P. Hexley, 2011 Red but not dead? Membranes of stressed
517 *Saccharomyces cerevisiae* are permeable to propidium iodide. *Environ Microbiol*
518 13 (1):163-171.
- 519 de Menezes, H.D., A.C. Pereira, G.T.P. Brancini, H.C. de Leao, N.S. Massola Junior *et*
520 *al.*, 2014 Furocoumarins and coumarins photoinactivate *Colletotrichum acutatum*

- 521 and *Aspergillus nidulans* fungi under solar radiation. *Journal of Photochemistry*
522 *and Photobiology B-Biology* 131:74-83.
- 523 de Menezes, H.D., L. Tonani, L. Bachmann, M. Wainwright, G.U. Braga *et al.*, 2016
524 Photodynamic treatment with phenothiazinium photosensitizers kills both
525 ungerminated and germinated microconidia of the pathogenic fungi *Fusarium*
526 *oxysporum*, *Fusarium moniliforme* and *Fusarium solani*. *J Photochem Photobiol*
527 *B* 164:1-12.
- 528 Gonzales, J.C., G.T.P. Brancini, G.B. Rodrigues, G.J. Silva-Junior, L. Bachmann *et al.*,
529 2017 Photodynamic inactivation of conidia of the fungus *Colletotrichum*
530 *abscissum* on *Citrus sinensis* plants with methylene blue under solar radiation. *J*
531 *Photochem Photobiol B* 176:54-61.
- 532 Köhler, J.R., A. Casadevall, and J. Perfect, 2015 The Spectrum of Fungi That Infects
533 Humans. *Cold Spring Harb Perspect Med* 5 (1).
- 534 Limper, A.H., A. Adenis, T. Le, and T.S. Harrison, 2017 Fungal infections in HIV/AIDS.
535 *Lancet Infect Dis* 17 (11):e334-e343.
- 536 Nishimoto, A.T., C. Sharma, and P.D. Rogers, 2020 Molecular and genetic basis of azole
537 antifungal resistance in the opportunistic pathogenic fungus *Candida albicans*. *J*
538 *Antimicrob Chemother* 75 (2):257-270.
- 539 Pavani, C., A.F. Uchoa, C.S. Oliveira, Y. Iamamoto, and M.S. Baptista, 2009 Effect of
540 zinc insertion and hydrophobicity on the membrane interactions and PDT activity
541 of porphyrin photosensitizers. *Photochem Photobiol Sci* 8 (2):233-240.
- 542 Perlin, D.S., R. Rautemaa-Richardson, and A. Alastruey-Izquierdo, 2017 The global
543 problem of antifungal resistance: prevalence, mechanisms, and management.
544 *Lancet Infect Dis* 17 (12):e383-e392.
- 545 Rashid, F., and R.W. Horobin, 1990 Interaction of molecular probes with living cells and
546 tissues. Part 2. A structure-activity analysis of mitochondrial staining by cationic
547 probes, and a discussion of the synergistic nature of image-based and biochemical
548 approaches. *Histochemistry* 94 (3):303-308.
- 549 Rhodes, J., and M.C. Fisher, 2019 Global epidemiology of emerging *Candida auris*. *Curr*
550 *Opin Microbiol* 52:84-89.
- 551 Rodrigues, G.B., M. Dias-Baruffi, N. Holman, M. Wainwright, and G.U. Braga, 2013 In
552 vitro photodynamic inactivation of *Candida* species and mouse fibroblasts with
553 phenothiazinium photosensitizers and red light. *Photodiagnosis Photodyn Ther* 10
554 (2):141-149.
- 555 Rodrigues, G.B., L.K. Ferreira, M. Wainwright, and G.U. Braga, 2012 Susceptibilities of
556 the dermatophytes *Trichophyton mentagrophytes* and *T. rubrum* microconidia to
557 photodynamic antimicrobial chemotherapy with novel phenothiazinium
558 photosensitizers and red light. *J Photochem Photobiol B* 116:89-94.
- 559 Scaduto, R.C., and L.W. Grotyohann, 1999 Measurement of mitochondrial membrane
560 potential using fluorescent rhodamine derivatives. *Biophys J* 76 (1 Pt 1):469-477.
- 561 Shor, E., and D.S. Perlin, 2015 Coping with Stress and the Emergence of Multidrug
562 Resistance in Fungi. *PLoS Pathog* 11 (3).
- 563 Tonani, L., N.S. Morosini, H. Dantas de Menezes, M.E. Nadaletto Bonifacio da Silva, M.
564 Wainwright *et al.*, 2018 In vitro susceptibilities of *Neoscytalidium* spp. sequence
565 types to antifungal agents and antimicrobial photodynamic treatment with
566 phenothiazinium photosensitizers. *Fungal Biol* 122 (6):436-448.
- 567 Wainwright, M., and R.M. Giddens, 2003 Phenothiazinium photosensitizers: choices in
568 synthesis and application. *Dyes and Pigments* 57 (3):245-257.
- 569 Wainwright, M., T. Maisch, S. Nonell, K. Plaetzer, A. Almeida *et al.*, 2017
570 Photoantimicrobials-are we afraid of the light? *Lancet Infect Dis* 17 (2):e49-e55.

- 571 Wainwright, M., K. Meegan, and C. Loughran, 2011 Phenothiazinium photosensitisers
572 IX. Tetra- and pentacyclic derivatives as photoantimicrobial agents. *Dyes and*
573 *Pigments* 91 (1):1-5.